Electron kinetics and non-Joule heating in near-collisionless inductively coupled plasmas

V. I. Kolobov
Plasma Processing Laboratory, Department of Chemical Engineering, University of Houston, Houston, Texas 77204-4792

D. P. Lymberopoulos
Applied Materials, 3100 Bowers Avenue, Santa Clara, California 95054

D. J. Economou
Plasma Processing Laboratory, Department of Chemical Engineering, University of Houston, Houston, Texas 77204-4792

(Received 1 July 1996)

Electron kinetics in an inductively coupled plasma sustained by a coaxial solenoidal coil is studied for the near-collisionless regime when the electron mean free path is large compared to the tube radius. Emphasis is placed on the influence of the oscillatory magnetic field induced by the coil current and the finite dimension of the plasma on electron heating and formation of the electron distribution function (EDF). A nonlocal approach to the solution of the Boltzmann equation is developed for the near-collisionless regime when the traditional two-term Legendre expansion for the EDF is not applicable. Dynamic Monte Carlo (DMC) simulations are performed to calculate the EDF and electron heating rate in argon in the pressure range 0.3–10 mTorr and driving frequency range 2–40 MHz, for given distributions of electromagnetic fields. The wall potential ϕ_w in DMC simulations is found self-consistently with the EDF. Simulation results indicate that the EDF of trapped electrons with total energy $\varepsilon < e\phi_w$ is almost isotropic and is a function solely of ε, while the EDF of untrapped electrons with $\varepsilon > e\phi_w$ is notably anisotropic and depends on the radial position. These results are in agreement with theoretical analysis. [S1063-651X(97)05403-2]

PACS number(s): 52.80.−s, 52.65.−y

I. INTRODUCTION

High-density plasmas operating at low gas pressures (<50 mtorr) have recently attracted considerable attention as primary candidates for the manufacturing of ultra-large-scale integrated circuits [1]. Inductively coupled plasma (ICP) sources are particularly attractive because of their relatively simpler design. Although ICPs have been known and studied for more than a century [2], the low-pressure operating regime desirable for modern microelectronics applications is historically unusual and has not been extensively explored until recently. Nonlocal electron kinetics is a distinctive feature of this regime. Most of the recent kinetic studies of low-pressure ICPs [3–5] have been limited to the collisional regime for which the electron mean free path λ is small compared to characteristic discharge dimensions. Modern applications, howerer, call for a plasma that is as free of collisions as possible. Collisionless electron heating and anomalous skin effect are typical of the near-collisionless operating regime, for which λ is larger than or comparable to the discharge dimensions. Interesting kinetic effects are caused by thermal motion of electrons in this regime.

Electron heating is one of the key processes that determine the power deposition and spatial uniformity of the plasma. Heating is a statistical process that transfers the directed energy acquired from the field into random energy of thermal motion. At high gas pressures, electron collisions with neutral atoms are responsible for this transfer; collisional (Joule) heating predominates. Heating at low pressures is due to a combined effect of electron interactions with the fields, reflections from the plasma boundaries (potential barriers), and collisions with gas species. Heating may occur even in the absence of collisions if there is a ''phase randomization'' mechanism that is equivalent to electron momentum transfer in collisions with gas species. Such collisionless (stochastic) electron heating is well known for capacitively coupled plasmas (CCPs) where it occurs due to electron interactions with oscillating sheath boundaries [6,7]. Between the two extremes of Joule heating and collisionless heating, there is an important regime of what we call ''hybrid'' heating. In the hybrid regime, an electron ''forgets'' the field phase due to collisions, but in contrast to Joule heating, hybrid heating is nonlocal: the place of the electron interaction with the field and the place where phase-randomizing collisions occur are separated in space. Generally, the behavior of electrons in this regime is governed by three frequencies: the frequency of the rf field ω, the collision frequency ν, and the bounce frequency Ω defined below. Depending on the relative magnitude of these frequencies, different electron dynamics and a variety of heating regimes can be distinguished. Both hybrid and collisionless heating belong to the category of non-Joule heating.

There is one property that fundamentally separates ICPs from CCPs. The magnetic field is a crucial factor for ICPs since its time variation induces an electric field that accelerates electrons. Contrary to the electric field in the CCP, the inductive electric field in the ICP is solenoidal, i.e., nonpotential in nature. The field lines are closed within the plasma and do not form oscillating sheaths as in CCPs. However, due to the nonpotential nature of the field, charged particles change energy in a round-trip through the field region even in the absence of collisions [8]. The existence of collisionless heating in the ICP was suggested by Godyak *et al.* [9] based on measurements of external electrical characteristics of an

inductive discharge. Turner [10] has drawn similar conclusions by calculating the surface impedance of a planar plasma slab using a particle-in-cell (PIC) Monte Carlo collisions simulation of electrons. He found that the real part of the surface impedance does not vanish with a reduction of gas pressure, indicating, in an indirect way, the existence of power absorption in the collisionless limit. An analytical model of electron heating was developed in [11] for a spatially homogeneous plasma with a Maxwellian electron distribution function. It was assumed that electrons interact with inductive electric field within a skin layer and, due to collisions with plasma species, forget the phase of the field between subsequent interactions. The model assumed implicitly that the electron mean free path does not exceed the characteristic dimension of the plasma so that any effects of finite size of the plasma could not be predicted.

In the near-collisionless operating regime, electron ''collisions'' with plasma boundaries (potential barriers) are more frequent than collisions with gas species. Under these conditions the finite dimensions of the plasma become an important consideration. The momentum gained by electrons from the electromagnetic forces in one place can be transferred by thermal motion to another place where the momentum may lead or lag the phase of the electric field, depending on the field frequency and transit time of electrons. Phase correlations and transit time resonances have a marked influence on the penetration of electromagnetic fields into a bounded plasma [12]. The influence of finite-size effects on electron heating was analyzed in [13] for a planar rf discharge. It was found that the mechanism of heating depends on the velocity component affected by the electron interaction with electromagnetic forces. The rf magnetic field in the ICP may have a major impact on this interaction.

Most papers on ICPs have neglected the influence of the oscillatory magnetic field B on electron motion. The possible influence of the B field on the anomalous skin effect in inductive discharges was mentioned by Demirkhanov *et al.* [14] more than 30 years ago. Recently, Cohen and Rognlien [15] have analyzed the influence of the B field on electron heating in ICPs. They pointed out that the Lorentz force due to the B field may exceed the electric force in the ICP. The Lorentz force changes the direction of the velocity kick an electron acquires in the skin layer. As a result, electron heating in the near-collisionless regime may be substantially different if the oscillatory magnetic field is accounted for in theoretical analysis or numerial modeling. Gibbons and Hewett [16] have observed in a PIC simulation that both electron velocity components in the plane orthogonal to B are affected by collisionless heating. Only the azimuthal component v_θ would have changed if the B field were neglected.

The purpose of the present paper is to analyze electron dynamics and the mechanism of electron heating in weakly collisional ICPs accounting for the oscillatory magnetic field and the finite dimensions of the plasma. The problem is treated analytically and numerically by using (a) integration of equations of single-particle motion, (b) approximate solution to the Boltzmann equation, and (c) dynamic Monte Carlo simulations. We have chosen a simple cylindrical system with prescribed profiles of the fields rather than solving the Maxwell equations self-consistently with electron kinetics. An analysis of the anomalous skin effect in ICPs is beyond the scope of this paper. It is known that penetration of electromagnetic fields into a bounded discharge plasma may be accompanied by nonmonotonic field profiles, resonance phemonena, etc. [14,17]. A review of classical and recent works on the anomalous skin effect can be found in Ref. [18].

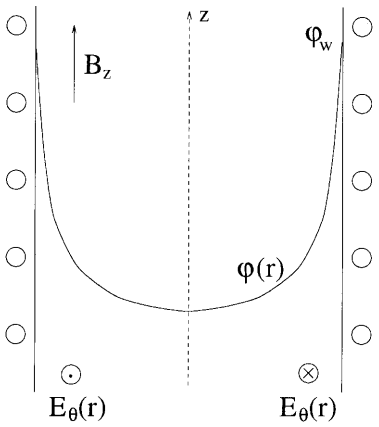

FIG. 1. Sketch of an inductive discharge with a coaxial solenoidal coil. A time-varying magnetic field B_z induces a solenoidal electric field E_θ. An electrostatic potential $\phi(r)$ is generated by the excess positive space charge. The depth of the potential well ϕ_w ensures the absence of a net charge flow to the dielectric wall of the chamber.

The structure of the paper is as follows. Section II presents an analysis of collisionless particle dynamics. The axial symmetry of the problem enables one to rely on the strict constancy of the canonical angular momentum to separate the radial and azimuthal motions. In Sec. III we develop a nonlocal approach to the solution of the Boltzmann equation for electrons in a near-collisionless ICP. Section IV describes the technique of dynamic Monte Carlo (DMC) simulation. The results of the DMC simulations in argon are presented in Sec. V for a wide range of discharge conditions. Section VI contains a discussion of the results.

II. COLLISIONLESS DYNAMICS OF CHARGED PARTICLES

Consider an inductively coupled plasma that is produced in a dielectric tube of radius R inserted into a long solenoidal coil (Fig. 1). The electric and magnetic fields induced by the rf current in the coil generally have both axial and circumferential components [19]. The axial component of the electric field E_z, which is due to the rf potential across the coil terminals, provides capacitive coupling. It can be eliminated or substantially reduced either by a metal screen or by an electrolyte enveroping the discharge vessel [20]. A time-varying magnetic field B_z gives rise to a solenoidal electric field E_θ according to Faraday's law. The E_θ field imparts kinetic energy on electrons and an inductive discharge can be sustained. Such electrodeless discharges (sometimes called ''ring discharges'') have a long and interesting history [2]. However, the low-pressure operating regime has not been thoroughly studied yet.

We are interested in the case when the mean free path of

plasma species exceeds the tube radius R, so that the particle motion is almost collisionless. Charged particles are accelerated in the azimuthal direction by the inductive electric field E_θ (Fig. 1). The B_z field produces a Lorentz force acting in the radial direction. When averaged over the rf period, this force attracts particles towards the axis regardless of the particle's charge. This ''radiation pressure'' effect is well known in high-temperature plasmas [21]. In addition to the rf fields, a substantial static space-charge electric field E_r is built up in the discharge. This field accelerates positive ions towards the wall and confines the majority of electrons in the plasma providing equality of charge flow to the dielectric wall of the chamber. The ion motion is a free fall. Electrons can escape the plasma after acquiring enough kinetic energy to overcome the potential barrier near the wall. At steady state, each electron during its lifetime must produce on average an electron-ion pair in ionization events.

A. Equations of motion

It is convenient to represent the space-charge field E_r by its scalar potential ϕ and to use the vector potential $\mathbf{A}$ for describing the alternating fields generated by the coil current. By virtue of azimuthal symmetry of the problem, the only nonvanishing component of $\mathbf{A}$ is the azimuthal component $A_\theta(r,t)$. Magnetic and electric rf fields are recovered from the relations $\partial(rA_\theta)/\partial r = rB_z$ and $-\partial A_\theta/\partial t = E_\theta$. These fields do not affect the particle motion along the z axis. Collisionless motion in the plane normal to B_z is governed by the Hamiltonian [21]

$$H=\frac{p_r^2}{2m}+\frac{1}{2m}\left(\frac{p_\theta - qrA_\theta}{r}\right)^2+q\phi(r), \tag{1}$$

where m and $q=\pm e$ are the mass and charge of a particle, r and θ are cylindrical coordinates, and p_r and p_θ are canonical momenta. Since the Hamiltonian (1) is independent of θ, the canonical angular momentum p_θ is an invariant of the motion:

$$p_\theta = mr^2\dot{\theta}+qrA_\theta = \text{const}. \tag{2}$$

Strict constancy of p_θ allows separating the radial and azimuthal motions. The angle $\theta(t)$ can be found from Eq. (2) if $r(t)$ and A_θ are known. On the other hand, the radial motion is independent of θ:

$$m\dot{r}=p_r, \tag{3}$$

$$\dot{p}_r=-q\frac{\partial\Psi}{\partial r}, \tag{4}$$

where

$$\Psi(p_\theta,r,t)=\frac{1}{2mq}\left(\frac{p_\theta - qrA_\theta}{r}\right)^2+\phi(r)=\frac{mv_\theta^2}{2q}+\phi(r) \tag{5}$$

is an effective potential. It is useful to separate Ψ into a time-independent part

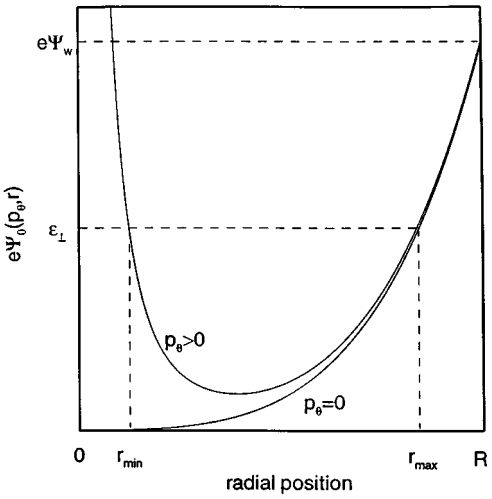

FIG. 2. Schematic of the effective potential $\Psi_0(r)$ [Eq. (6)] for $p_\theta>0$ and for $p_\theta=0$. $r_{\min}$ and $r_{\max}$ indicate coordinates of turning points for an electron with energy $\varepsilon_\perp$.

$$\Psi_0(p_\theta,r)=\frac{p_\theta^2}{2mqr^2}+\frac{q\langle A_\theta^2\rangle}{2m}+\phi(r) \tag{6}$$

and an alternating part

$$\Psi_1=-\frac{p_\theta A_\theta}{mr}-\frac{q}{2m}(A_\theta^2-\langle A_\theta^2\rangle). \tag{7}$$

Here $\langle A_\theta^2\rangle$ denotes the time-averaged value of $A_\theta^2(r,t)$ (the time-average of A_θ is zero). The first term on the right-hand side of Eq. (6) is due to the centrifugal force, i.e., an effective force in the r direction resulting from particle motion in the θ direction. The second term on the right-hand side of Eq. (6) is the pondermotive or Miller force that describes ''radiation pressure'' [21]. Radiation pressure forces both electrons and ions from regions of high rf field into regions of weaker field, i.e., towards the tube axis. Since the Miller force is inversely proportional to particle mass, its influence on ions is typically negligible compared to the electrostatic force, which accelerates ions towards the wall.

For electrons, the alternating part of the potential Ψ_1 may be considered as a small perturbation at relatively high frequencies. In the high-frequency limit, the perpendicular energy of electrons

$$\varepsilon_\perp = m\dot{r}^2/2+e\Psi_0(p_\theta,r) \tag{8}$$

is a constant of the motion and there is no electron heating. The potential Ψ_0 confines the majority of electrons in the plasma. Setting $v_r=0$ determines, for each set of $\varepsilon_\perp$ and p_θ, the coordinates of two turning points $r_{\min}$ and $r_{\max}$ (Fig. 2). The period of bounce oscillations

$$T(\varepsilon_\perp,p_\theta)=2\int_{r_{\min}}^{r_{\max}}\frac{dr}{\sqrt{2[\varepsilon_\perp - e\Psi_0(p_\theta,r)]/m}} \tag{9}$$

and the bounce frequency $\Omega(\varepsilon_\perp,p_\theta)=2\pi/T$ are functions of electron energy $\varepsilon_\perp$ and angular momentum p_θ.

B. Low-density plasmas

Electromagnetic fields in ICPs are spatially inhomogeneous even in the absence of a skin effect. To distinquish finite-size effects and the field shielding by the plasma, let us consider the collisionless skin depth $\delta = c/\omega_p$, where ω_p is the electron plasma frequency and c is the speed of light. For $n_e = 10^{10}$ cm^{-3}, $\delta = 5$ cm, which is equal to the radius of the tube R considered in this paper. At low plasma density, when $\delta > R$, the skin effect is negligible. (Simple estimates indicate that the ambipolar diffusion regime is established long before the field shielding begins.) In any case, however, E_θ must vanish on the axis due to azimuthal symmetry of the problem. In the absence of skin effect, the rf current in the coil with angular frequency ω produces electromagnetic fields with the vector potential

$$A_\theta = A_0(r)\sin\omega t = (B_0 r/2)\sin\omega t, \tag{10}$$

which corresponds to a spatially uniform magnetic field

$$B_z = B_0 \sin\omega t \tag{11}$$

and linearly varying electric field

$$E_\theta = -(E_0 r/R)\cos\omega t \tag{12}$$

of amplitude $E_0 = B_0 \omega R/2$. The ratio of the electric force eE_θ to the magnetic (Lorentz) force evB is $\omega r/2v$. This ratio decreases with a decrease of ω and can be rather small at low frequencies even at $r = R$. The magnetic field can therefore have considerable impact on electron dynamics.

Consider collisionless electron motion under the influence of the rf fields (11) and (12) and an electrostatic field $E_r = -d\phi/dr$. A similar problem was treated by Weibel [22], who analyzed stable orbits of charged particles in electromagnetic fields of a circular waveguide [when $A_0(r)$ is a Bessel function] for $\phi = 0$. In our case, the first term of Ψ_1 gives no contribution to the force and the equations of motion (3)–(5) are reduced to

$$\ddot{r} = \frac{p_\theta^2}{m^2 r^3} - \left(\frac{\omega_L}{2}\right)^2 r\sin^2\omega t - \frac{eE_r}{m}, \tag{13}$$

where $\omega_L = eB_0/m$ is the Larmor frequency. For the particularly simple case $E_r(r) = E_0 r/R$, Eq. (13) is equivalent to a set of two completely decoupled equations for $x = r\cos\theta$ and $y = r\sin\theta$, both of the Mathieu type

$$\{\ddot{x},\ddot{y}\} = -\Omega^2\left(1 - \frac{\omega_L^2}{8\Omega^2}\cos 2\omega t\right)\{x,y\}. \tag{14}$$

Equation (14) describes a linear oscillator under the influence of a harmonic external force of frequency 2ω. The frequency of natural oscillations $\Omega = (\omega_L^2/8 + eE_0/mR)^{1/2}$ is independent of energy. A parametric resonance is known to occur when the frequency of the force (2ω) is close to $k\Omega$, where k is an integer. For $\Omega = \omega_L/\sqrt{8}$ (no electrostatic field), the basic resonance $(k = 1)$ takes place in the interval [22]

$$1.15 < (\omega_L/2\omega) < 1.89. \tag{15}$$

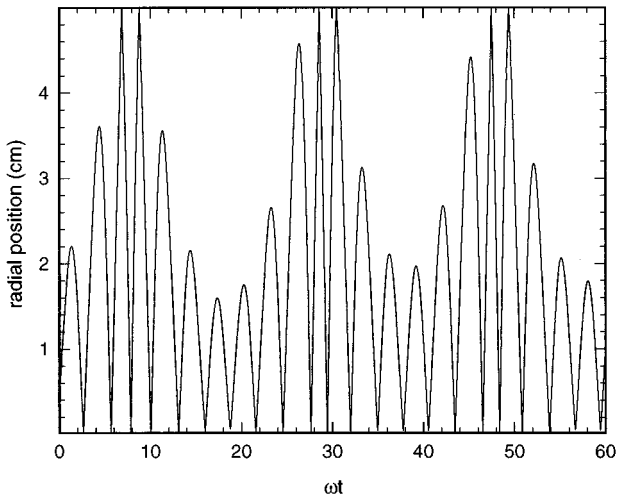

FIG. 3. Radial electron position as a function of time for resonance conditions $B = 1$ G, $\omega = 7\times10^6$ s^{-1} (1.1 MHz), and $\omega_L/2\omega = 1.27$, $p_\theta = 0.1 m\omega R^2$, $R = 5$ cm. A rectangular potential well was assumed. The time modulation of the amplitude of bounce oscillations corresponds to phase oscillations of the electron energy with respect to the electric field.

This resonance may have a major impact on gas breakdown in inductive discharges.

The resonance between bounce oscillations and rf fields can rapidly accelerate electrons. The amplitude of electron oscillations increases with time (Fig. 3). Under breakdown conditions $(\phi = 0)$, electrons would escape to the wall when the amplitude of their bounce oscillations equals the tube radius. In a discharge, the potential $\phi(r)$ is nonparabolic in the vicinity of the wall due to the presence of a space-charge sheath. Equation (14) is no longer valid at that location. Due to electron reflection from the sheath, the bounce frequency Ω becomes a function of electron energy. That detunes the frequency, generally leading to phase oscillations with respect to the field (see Fig. 3). The variations of the bounce amplitudes shown in Fig. 3 correspond to variations of electron energy with time. Under the conditions of Fig. 3, the limited energy excursions correspond to regular electron motion. Under certain conditions, due to the nonlinearity of oscillations [the dependence of Ω on $\varepsilon_\perp$ in Eq.(9)], the motion of electrons may become chaotic. That corresponds to the onset of collisionless heating. We shall illustrate the origin of the chaos and the appearance of collisionless heating for the more practical case of a thin skin layer, which is analyzed in the next subsection.

C. High-density plasmas

For high-density plasmas with $\delta \ll R$, the rf fields are localized within a thin skin layer near the wall. Electromagnetic forces act impulsively rather than continuously on bouncing electrons. Since $\delta \ll R$, one can neglect the time $\tau = 2\delta/v_r$ electrons spend in the skin layer compared to the bounce time $t_{n+1} - t_n$ between two sequential interactions. In the presence of an electrostatic potential in the plasma, only sufficiently energetic electrons are capable of overcoming the potential barrier and reach the skin layer. For these electrons one can neglect the influence of the electrostatic potential for calculation of the bounce period from Eq. (9):

$$T=\frac{R}{\varepsilon_\perp}\sqrt{2m\varepsilon_\perp-\left(\frac{p_\theta}{R}\right)^2}. \tag{16}$$

Due to the two-dimensional nature of the problem, the period T is a function of two variables p_θ and $\varepsilon_\perp$. The period T vanishes for particles with $p_r=0$ moving along a circle of radius $r\approx R$. Another limiting case, namely, $p_\theta=0$, resembles a planar geometry. For $p_\theta\neq 0$, the period T has a maximum with respect to $\varepsilon_\perp$. Due to strict constancy of the canonical momentum p_θ, a change in $\varepsilon_\perp$ in the skin layer corresponds to a change in radial electron velocity. Thus, in the limiting case $\delta\ll R$, electron interactions with the rf fields affect only the radial part of electron energy.

Let us construct a mapping relating the values of variables between sequential interactions. Let ξ_n designate the phase of the field ($\xi_n=\omega t_n$) at the moment of the nth electron reflection from the plasma boundary at $r=R$. The phases of the field between two sequential interactions are given by

$$\xi_{n+1}=\xi_n+\omega T(\varepsilon_{n+1}). \tag{17}$$

Integrating the equations of motion in the skin layer yields

$$\varepsilon_{n+1}=\varepsilon_n+Q(\xi_n), \tag{18}$$

where $\varepsilon_{n+1}=\varepsilon(t_{n+1}-\tau)$ and $\varepsilon_n=\varepsilon(t_n-\tau)$ are radical electron energies before the $n+1$ and n kicks, respectively. The energy change in the skin layer Q is proportional to the power (the product of force $e\partial\Psi_1/\partial r$ and electron velocity $\dot{r}$) evaluated along a trajectory [23]

$$Q=e\int_{t_n-\tau}^{t_n+\tau}\dot{r}\frac{\partial\Psi_1(r(t),t)}{\partial r}dt. \tag{19}$$

The difference equations (17) and (18) are equivalent to the equations of motions (3) and (4). The value of the derivative $d\xi_{n+1}/d\xi_n$ defines the degree of phase correlations. The inequality

$$\left|\frac{d\xi_{n+1}}{d\xi_n}-1\right|\geqslant 1 \tag{20}$$

serves as a rough criterion of local phase instability [23]. If Eq. (20) holds true, electron trajectories become chaotic in spite of the fact that the equations of motion contain no random forces. In some sense, the chaotic component of the motion remains weak compared to the regular component: it manifests itself on larger spatial and time scales in comparison to the regular bounce motion. Chaotic dynamics corresponds to ''slow'' electron diffusion along the ''energy axis'' from regions in phase space where particles are abundant to regions where particle density is low. Since the electron distribution function (EDF) usually decreases with energy, such a diffusion corresponds to collisionless electron heating.

Using Eqs. (20) and (16) and taking into account only the linear term of Ψ_1 in Eq. (7), one obtains from Eq. (20)

$$\frac{\omega T\Delta\varepsilon}{\varepsilon}\frac{|(p_\theta/R)^2-m\varepsilon|}{2m\varepsilon-(p_\theta/R)^2}\geqslant 1, \tag{21}$$

where $\Delta\varepsilon$ is the magnitude of the energy kick. The phase of the rf field appears to be random for electrons if small changes of electron energy in the skin layer result in considerable changes in phase. In the vicinity of the maximum of $T(\varepsilon)$, where T is weakly energy dependent, small changes in $T(\varepsilon)$ also result in a small change in the phase over the period of bounce oscillations. The heating becomes second order with respect to $\Delta\varepsilon$. On the contrary, for $T\to 0$, where the derivative $dT/d\varepsilon$ tends to infinity, even small changes in energy may result in considerable changes in phase; the denominator of Eq. (21) becomes zero. Far from these peculiarities, which are specific to cylindrical geometry, inequality (21) requires that $\omega T\Delta\varepsilon/\varepsilon>1$. This condition, well known for a planar case [24], states that for small-amplitude kicks $\Delta\varepsilon$, the driving frequency ω must be sufficiently large so that the field could change many times during the bounce period. For small p_θ (as in the planar case), the bounce period T decreases with an increase in energy and the motion of energetic electrons is more regular. Equation (21) imposes restrictions on the maximum energy electrons can achieve by the collisionless heating mechanism.

To proceed further, we have to calculate the energy kick per single pass through the skin layer. For the sake of simplicity, let us assume, as in [11,15], an exponential decay of the fields within the skin layer: $A_\theta=A_0\exp[-(R-r)/\delta]$. For $Q\ll\varepsilon$, integrating along unperturbed trajectories $\dot{r}=\pm v_r t$, we obtain [11,15]

$$Q(p_\theta,p_r,\xi)=\omega_L\delta\sin\xi(2p_\theta/R+m\omega_L\delta\cos\xi)\frac{\omega\tau}{1+(\omega\tau)^2}, \tag{22}$$

where $\omega_L=eB_0/m$ is the Larmor frequency in the magnetic field $B_0=A_0/\delta$. Two points are worth mentioning regarding Eq. (22). (a) Evidently, the maximal energy can be acquired if the electric field remains in the same direction during the entire electron transit through the skin layer. However, since the amplitude of the induced electric field ($E_\theta\propto\omega$) decreases with ω, the optimal conditions for the energy gain take place at $\omega\tau=1$ when Q reaches a maximum with respect of $\omega\tau$. (b) The term of Q linear with respect to $\omega_L\delta$ vanishes for $p_\theta=0$ due to symmetry of the problem.

The important difference of our analysis from [11], where the rf magnetic field was neglected, is in the direction of the velocity kick. Accounting for the magnetic field results in a velocity kick normal to the plasma boundary, similar to that taking place in a capacitively coupled rf discharge [15]. The direction of the velocity kick greatly influences the dynamics of bouncing electrons; for instance, in the planar case, kicks parallel to the boundary (as in [11]) imply the absence of collisionless heating [13]. Contrary to the capacitively coupled plasma, electrons entering the skin layer with zero azimuthal velocity experience no energy kick in the linear approximation: the first term in Eq. (22) vanishes for $p_\theta=0$. In the linear approximation, the mapping (17) and (18) can be written in the form

$$\mathcal{E}_{n+1}=\mathcal{E}_n+\frac{4\omega_L}{\omega}P\sin\xi_n\frac{\sqrt{\mathcal{E}_n}}{\mathcal{E}_n+1}, \tag{23}$$

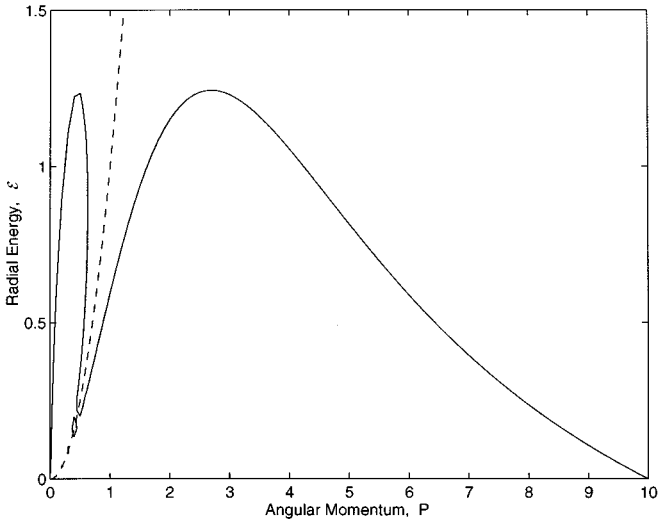

FIG. 4. Regions of regular (above) and chaotic (below solid lines) electron dynamics for the case of a thin skin layer. The solid lines indicate the maximal values of the radial electron energy $\mathcal{E}$ that can be reached in collisionless heating for a particular value of the angular momentum P.

$$\xi_{n+1}=\xi_n+\frac{2R}{\delta}\frac{\sqrt{\mathcal{E}_{n+1}}}{\mathcal{E}_{n+1}+P^2}+\frac{2\omega_L}{\omega}P\cos\xi_n\frac{\mathcal{E}_{n+1}-1}{(\mathcal{E}_{n+1}+1)^2\sqrt{\mathcal{E}_{n+1}}}, \tag{24}$$

where $P=p_\theta/m\omega\delta R$ and $\mathcal{E}=2\varepsilon/m(\omega\delta)^2-P^2$ are dimensionless momentum and energy, respectively. Since the transformation from n to $n+1$ is generated by Hamilton's equations, the mapping (23) and (24) must be area preserving. The last term in Eq. (24) accounts for the first-order change in phase to ensure area preservation [24]. In variables $\mathcal{E}$ and P, the boundary of chaos defined by Eq. (21) becomes

$$\frac{4\omega_L R}{\omega\delta}\frac{P\sqrt{\mathcal{E}}|P^2-\mathcal{E}|}{(\mathcal{E}+1)(\mathcal{E}+P^2)^2}>1. \tag{25}$$

This boundary is shown in Fig. 4 for typical discharge conditions, $\omega=8.5\times10^7$ s^{-1} (13.56 MHz), $\omega_L=1.7\times10^7$ s^{-1} ($B_0=1$ G), $\delta=1$ cm, and $R=5$ cm. The dashed line corresponds to the maximum of $T(\mathcal{E})$, where heating becomes second order with respect to $\Delta\varepsilon$. Since collisionless heating affects only the radial part of electron energy, electrons can be heated up to radial energies $m(\omega\delta)^2/2\sim2$ eV for the conditions of Fig. 4. An increase of ω_L or a decrease of ω leads to an increase of these energies.

III. BOLTZMANN EQUATION FOR ELECTRONS

The electron distribution function in a rf discharge is a function of time, three electron velocities, and (at least one) spatial coordinate. In general, the solution of the Boltzmann equation for the EDF is a formidable numerical task. For that reason, the development of reliable approximations is valuable. The traditional two-term Legendre expansion of the EDF is valid only for the collisional regime $\lambda\ll R$ [25]. However, due to the large difference between momentum and energy relaxation rates of electrons, a separation of the EDF into two parts can be performed for the free-flight regime as well [26,27]. In rf discharges, one can separate rapidly and slowly varying parts of the EDF. For trapped electrons, the slowly varying part turns out to be almost isotropic. Furthermore, by performing an appropriate spatial averaging, the kinetic equation for the isotropic part is reduced to an ordinary differential equation. Thus, for the majority of electrons, the principal part of the EDF turns out to be a function of a sole variable, the total electron energy.

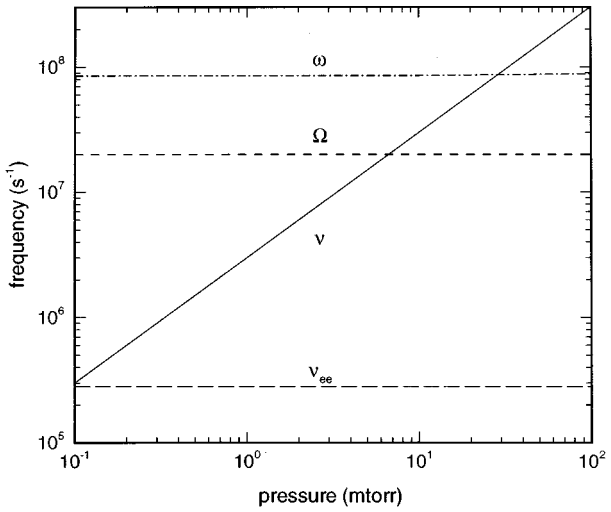

FIG. 5. Characteristic frequencies for an argon discharge for electrons with an energy of 5 eV, a plasma density of 10^{11} cm^{-3}, and the tube radius $R=5$ cm: angular frequency ω, bounce frequency Ω, transport collision frequency ν, and the frequency of Coulomb interaction among electrons ν_{ee}.

A. Nonlocal approach

It is convenient to use invariants of the particle motion as independent variables in the Boltzmann equation. Taking advantage of the azimuthal symmetry of our problem and using the canonical momentum p_θ as an independent variable, the Boltzmann equation for electrons can be written in the form [25]

$$\frac{\partial f}{\partial t}+v_r\frac{\partial f}{\partial r}+\dot{p}_r\frac{\partial f}{\partial p_r}=S, \tag{26}$$

where S is a collision operator and $\dot{p}_r$ is given by Eq. (4). The electron distribution function f in Eq. (26) is a function of p_r, p_θ, p_z, r, and t. Since there is no variation with z and θ, these coordinates have been omitted. Also, the term $\dot{p}_\theta\partial f/\partial p_\theta$ vanishes because $\dot{p}_\theta=0$ [see Eq. (2)]. According to Eq. (26), electron motion along z is coupled to the motion in the (x,y) plane solely due to collisions.

The ICP is a weakly ionized plasma. For the majority of electrons, the frequency of electron collisions with neutral atoms exceeds the frequency of Coulomb interactions among electrons (see Fig. 5). In the pressure range of interest, the bounce frequency Ω exceeds the momentum transfer collision frequency ν. In argon (as in many other gases) the total frequency of inelastic collisions ν^* (which includes excitation and ionization of atoms) is small compared to ν in the

energy range of interest. The difference between ν and ν^* (i.e., the difference between momentum and energy relaxation rates) can be used to simplify the Boltzmann equation.

Let us rewrite Eq. (26) using the transverse energy $\varepsilon_\perp$ [Eq. (8)] as an independent variable

$$\frac{\partial f}{\partial t}+v_r\left(\frac{\partial f}{\partial r}\right)_{\varepsilon_\perp}-e\frac{\partial \Psi_1}{\partial r}v_r\frac{\partial f}{\partial \varepsilon_\perp}=-\nu(f-F_0)+S^*. \tag{27}$$

Now, the EDF is a function of $\varepsilon_\perp, p_\theta, p_z, r$, and t, while the radial electron velocity $v_r=\sqrt{2(\varepsilon_\perp-e\Psi_0)/m}$ is a function of independent variables. The first term on the right-hand side of Eq. (27) describes momentum transfer in collisions with gas species. The scattering is assumed to be isotropic and F_0 designates the isotropic part of the EDF

$$F_0(\varepsilon)=\frac{1}{4\pi}\int f d\Omega_v, \tag{28}$$

which is assumed time independent for reasons discussed below. Integration in Eq. (28) is performed over angles in velocity space and $\varepsilon=\varepsilon_\perp+p_z^2/2m$ denotes the total energy. The term S^* on the right-hand side of Eq. (27) describes inelastic processes such as excitation and ionization of atoms, excitation of molecular vibrations and rotations, energy loss in elastic collisions with atoms, and Coulomb interactions among electrons. These processes can be divided into quasielastic and substantially inelastic. Quasielastic processes, such as excitation of molecular vibrations and rotations, energy loss in elastic collisions with atoms, and Coulomb interactions among electrons, can be written in a Fokker-Planck form [25]. Substantially inelastic processes correspond to removing high-energy electrons and replacing them by low-energy ones. For instance, excitation of a single atomic level with energy ε^* is described by

$$S_1^*=-\nu_1^*(\varepsilon)f+\sqrt{\frac{\varepsilon'}{\varepsilon}}\nu_1^*(\varepsilon')f(\varepsilon'). \tag{29}$$

In this process a high-energy electron loses an energy quantum ε^* and reappears at energy $\varepsilon'=\varepsilon-\varepsilon^*$. Let ν^* designate the frequency of all substantially inelastic processes including ionization. For most gases $\nu\gg\nu^*$ in the considered energy range. Also, for plasma densities typical to ICPs, $\nu\gg\nu_{ee}$ for the majority of electrons (see Fig. 5). Thus the inelastic collision term S^* in Eq. (27) is usually small compared to νf.

The EDF may be expressed as the sum of a rapidly varying part f_1 and a slowly varying part f_0. The latter is almost time independent for $\omega\gg\nu^*$ [25]. The equation for f_1 is

$$\frac{\partial f_1}{\partial t}+v_r\left(\frac{\partial f_1}{\partial r}\right)_{\varepsilon_\perp}-e\frac{\partial \Psi_1}{\partial r}v_r\frac{\partial f_0}{\partial \varepsilon_\perp}=-\nu f_1. \tag{30}$$

The equation for $f_0(\varepsilon_\perp, p_\theta, p_z, r)$ is

$$v_r\left(\frac{\partial f_0}{\partial r}\right)_{\varepsilon_\perp}-\left\langle e\frac{\partial \Psi_1}{\partial r}v_r\frac{\partial f_1}{\partial \varepsilon_\perp}\right\rangle=-\nu(f_0-F_0)+S^*, \tag{31}$$

where the angular brackets designate time averaging over a rf period

$$\langle f\rangle=f_0=\frac{\omega}{2\pi}\int_0^{2\pi/\omega}f\,dt. \tag{32}$$

For the majority of electrons, the difference, f_0-F_0, is expected to be rather small, so that the energy relaxation term S^* in Eq. (31) may exceed $\nu(f_0-F_0)$.

The first two terms of Eq. (30) are recognized as the total time derivative in configuration space. Thus the solution of Eq. (30) can be found by integration along electron trajectories [12]

$$f_1=e\int_0^\infty ds\; e^{-\nu s}v_r(t-s)\frac{\partial \Psi_1}{\partial r}[r(t-s),t-s]\frac{\partial f_0}{\partial \varepsilon_\perp}. \tag{33}$$

Having expressed the alternating part f_1 in terms of the main part f_0, we may substitute Eq. (33) into Eq. (31) to obtain an equation for f_0

$$v_r\left(\frac{\partial f_0}{\partial r}\right)_{\varepsilon_\perp}-v_r\frac{\partial}{\partial \varepsilon_\perp}J_\varepsilon(\varepsilon_\perp,r,p_\theta)=-\nu(f_0-F_0)+S^*, \tag{34}$$

where

$$J_\varepsilon=e^2\int_0^\infty ds\; e^{-\nu s}\left\langle\frac{\partial \Psi_1}{\partial r}v_r(t-s)\frac{\partial \Psi_1}{\partial r}[r(t-s),t-s]\right\rangle\frac{\partial f_0}{\partial \varepsilon_\perp} \tag{35}$$

is the electron flux along the $\varepsilon_\perp$ axis caused by electron heating.

Consider trapped electrons with $\varepsilon_\perp<e\phi_w$. The bounce motion of these electrons [described by the first term of Eq. (34)] occurs much more rapidly than their displacement along the energy axis; the first term in Eq. (34) dominates. This term vanishes if f_0 does not depend explicitly on r, i.e., if $f_0=F(\varepsilon_\perp, p_\theta, p_z)$. An equation for F can be obtained by dividing Eq. (34) by v_r and integrating over the discharge cross section accessible to electrons with energy $\varepsilon_\perp$. This procedure of spatial averaging results in [26]

$$\frac{\partial}{\partial \varepsilon_\perp}D(\varepsilon_\perp,p_\theta)\frac{\partial F}{\partial \varepsilon_\perp}=\overline{\nu}(F-F_0)-\overline{S^*}, \tag{36}$$

where

$$D=e^2\Omega\int_{r_{\min}}^{r_{\max}}\frac{dr}{v_r}\int_0^\infty ds\; e^{-\nu s}\times\left\langle\frac{\partial \Psi_1}{\partial r}v_r(t-s)\frac{\partial \Psi_1}{\partial r}[r(t-s),t-s]\right\rangle \tag{37}$$

is the energy diffusion coefficient and Ω is the bounce frequency for an electron with energy $\varepsilon_\perp$ and canonical momentum p_θ. The overbar denotes spatial averaging:

$$\overline{g}=\Omega\int_{r_{\min}}^{r_{\max}}\frac{g}{v_r}dr. \tag{38}$$

Equation (36) describes a complex process of energy redistribution between three degrees of freedom. Heating produces an electron flux along the $\varepsilon_\perp$ axis towards high energies and thus causes a departure of the EDF from an isotropic one. Elastic collisions tend to restore the isotropy of the EDF. They act on a time scale that is long compared to the bounce time, but short compared to the electron lifetime, resulting in an almost isotropic distribution of trapped electrons. When $\nu \gg \nu^*$ holds true, Eq. (36) can be simplified even further. The EDF can be written as the sum of an isotropic part F_0 and a small anisotropic addition $F_1 \ll F_0$: $F(\varepsilon_\perp, p_\theta, p_z) = F_0(\varepsilon) + F_1(\varepsilon_\perp, p_\theta, p_z)$. The equation for the isotropic part has the form

$$\frac{d}{d\varepsilon} D_\varepsilon(\varepsilon) \frac{dF_0}{d\varepsilon} = -\overline{S^*}, \tag{39}$$

where $D_\varepsilon(\varepsilon)$ is the energy diffusion coefficient averaged over p_θ and p_z:

$$D_\varepsilon(\varepsilon) = \frac{1}{2m\varepsilon} \int \int_{p_\theta^2 + p_z^2 < 2m\varepsilon} D(\varepsilon_\perp, p_\theta) dp_\theta dp_z. \tag{40}$$

The energy diffusion coefficient D_ε contains all information about electron heating and determines microscopic characteristics of the electron ensemble such as the principal part of the EDF, F_0, and macroscopic quantities such as the rate of power deposition into the plasma.

Thus, similar to the collisional case $\lambda < \delta$ [3,4], electrons are separated into two groups with respect to total energy: trapped electrons with $\varepsilon < e\phi_w$ and ''free'' electrons with $\varepsilon > e\phi_w$. For trapped electrons, the kinetic equation is reduced to an ordinary differential equation, Eq. (39). For free electrons, the more general equation, Eq. (34), should be used. These electrons are capable of escaping the discharge and their EDF depends explicitly on radial position. Moreover, at $\lambda > R$, the EDF of free electrons becomes notably anisotropic. While in the collisional case $\lambda < R$ considerable anisotropy of the EDF appears only at a distance approximately equal to λ near the wall (due to the absence of electron flux from the wall), in the free-flight case the EDF anisotropy manifests itself everywhere. Since only those electrons for which $v_r(\varepsilon_\perp, p_\theta, R) > 0$ can escape to the wall, the velocity of an escaping electron must satisfy the condition

$$\varepsilon_\perp - \frac{p_\theta}{mR^2} > e\phi_w. \tag{41}$$

Thus electrons with $p_\theta \approx 0$ that move away from the axis can escape if $\varepsilon_\perp > e\phi_w$. Since these electrons are present only in the vicinity of the axis, the EDF at $r \approx 0$ decreases rapidly with energy starting at $\varepsilon_\perp \approx e\phi_w$. For larger r, such a decrease of the EDF begins at higher $\varepsilon_\perp$. Consequently, the EDF at $\varepsilon_\perp > e\psi_w$ becomes a complicated function of radial position and angles. While free electrons are primarily responsible for the dc component of the electron current and give considerable contribution to the energy balance at low pressures, their contribution to average quantities such as electron density, temperature, and power deposition is, in general, negligible.

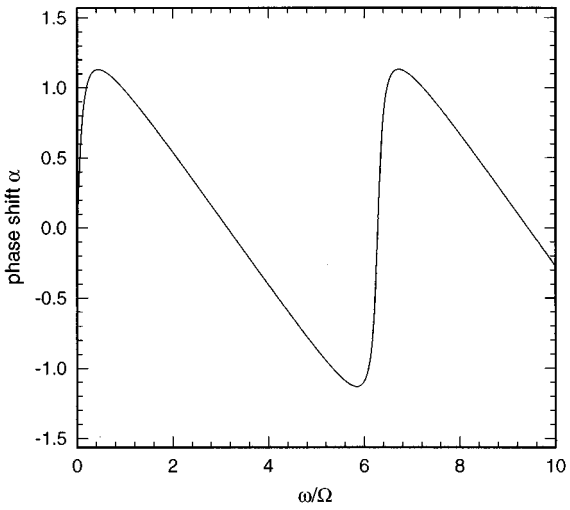

FIG. 6. Phase shift α between oscillations of the EDF f_1 and oscillations of the accelerating force [Eq. (43)].

B. Energy diffusion coefficient for a thin skin layer

The induced electric field in a cylindrical ICP is spatially inhomogeneous even in the absence of the skin effect (see Fig. 1). The magnetic field becomes spatially inhomogeneous only due to the field shielding by the plasma. For $\delta < R$, we consider only the linear term of Ψ_1 in Eq. (7), which gives the principal contribution to the electromagnetic force for electrons with nonzero p_θ. In the limiting case of a thin skin layer $\delta \ll R$, retaining only the linear term of Q in Eq. (22), integration of Eq. (33) can be carried out to give the oscillating part of the EDF in the form

$$f_1(\varepsilon_\perp, p_\theta, t) = \Delta\varepsilon \frac{\partial f_0}{\partial \varepsilon_\perp} \sum_{n=0}^{\infty} e^{-\nu t_n} \sin\omega(t - t_n). \tag{42}$$

Here $\Delta\varepsilon$ is the energy kick in one pass through the skin layer and t_n designates the time of the nth electron interaction with the skin layer. Consider the hybrid regime when chaotization of electron motion is due to collisions [13]. For this regime, using the approximation $t_n \approx 2\pi n/\Omega$, we find

$$f_1 = \frac{\Delta\varepsilon}{2} \frac{\partial f_0}{\partial \varepsilon_\perp} \{\Phi_1(x,y)\sin\omega t - \Phi_2(x,y)\cos\omega t\}, \tag{43}$$

where $x = 2\pi\omega/\Omega$, $y = 2\pi\nu/\Omega$, and functions Φ_1 and Φ_2 are defined as

$$\Phi_1 = \frac{\exp y - \cos x}{\cosh y - \cos x}, \tag{44}$$

$$\Phi_2 = \frac{\sin x}{\cosh y - \cos x}. \tag{45}$$

The function f_1 oscillates with frequency ω and with a phase shift $\alpha = \arctan(\Phi_2/\Phi_1)$ with respect to the oscillations of the force $\partial\Psi_1/\partial r \propto \sin\omega t$. The phase shift α is small at high pressures, when $\nu \gg \Omega$. At low pressures, in the near-collisionless regime ($\nu \ll \Omega$) the phase shift α is a periodic function of x with a period 2π (see Fig. 6). Under resonance conditions, the amplitude of f_1 may be quite large due to

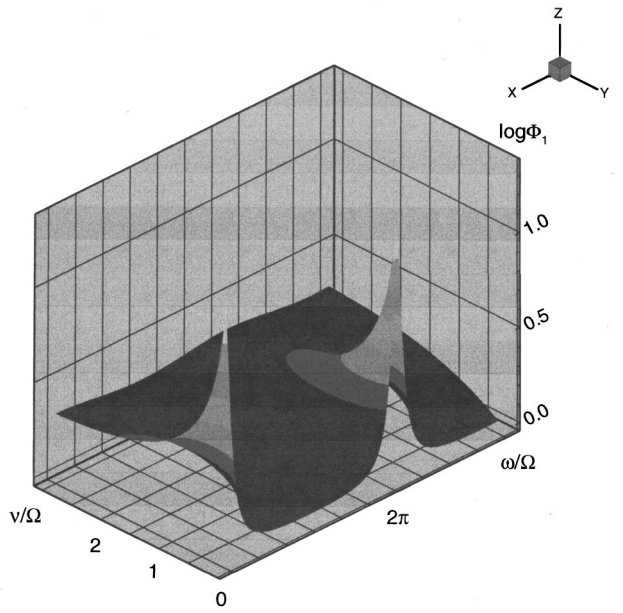

FIG. 7. Function Φ_1 [Eq. (43)] that describes phase correlations for hybrid heating regime. Strong resonances between bounce oscillations and rf fields are observed in the near-collisonless regime ($\nu \ll \Omega$) at $\omega = k\Omega$, where $k = 0, 1, 2, \ldots$.

strong correlations of the field phases and large energy excursion compared to energy kick $\Delta\varepsilon$ per single pass through the skin layer.

The second term of f_1, shifted in phase by $\pi/2$ with respect to the force, produces no work when averaged over one period. Only the first term contributes to the power absorption in the plasma. From Eqs. (37) and (43), the energy diffusion coefficient for the hybrid heating regime is

$$D = \frac{1}{2}(\Delta\varepsilon)^2 \Omega \Phi_1(x,y). \tag{46}$$

In limiting cases, this energy diffusion coefficient was obtained in Ref. [13] for a planar geometry. The energy diffusion coefficient is a product of a single energy kick in the skin layer, the bounce frequency Ω, and the function Φ_1, which describes the phase correlations between successive kicks. At $y \ll 1$, function $\Phi_1(x,y)$ exhibits resonances at $x = 2\pi k$, where k is an integer (see Fig. 7). The energy diffusion coefficient

$$D = \frac{(\Delta\varepsilon)^2}{2}\Omega\left[1 + \frac{1}{\pi}\frac{\nu\Omega}{\nu^2 + (2\Omega/\pi)^2[1-\cos(2\pi\omega/\Omega)]}\right] \tag{47}$$

is anomalously large for resonant particles with $\omega \approx k\Omega$. For $\nu \to 0$, D tends to a δ function. Far from resonances, the second term in the set of large square brackets of Eq. (47) is small. At low excitation frequencies $\omega^2 \ll 2\nu\Omega$, the energy diffusion coefficient (46) also reaches a maximum due to phase correlations of the rf field with respect to electron motion

$$D = \frac{(\Delta\varepsilon)^2 \nu \Omega^2}{\omega^2 + \nu^2}. \tag{48}$$

In the case of frequent collisions $\nu \gg \Omega$, the energy diffusion coefficient (46) is particularly simple

$$D = (\Delta\varepsilon)^2 \Omega. \tag{49}$$

It is interesting to note that the collision frequency ν does not appear explicitly in Eq. (49) even though collisions are responsible for phase randomization.

For collisionless heating, the energy diffusion coefficient can be obtained using a random-phase approximation [13]. The resulting expression for D coincides with Eq. (49). Although the mechanism of phase randomization is different in the collisionless and hybrid regimes, the heating rate described by Eq. (49) turns out to be the same. This is due to the fact that, for the considered hybrid regime, only electrons at a distance λ from the skin layer participate in the heating process.

The energy diffusion coefficients given by Eqs. (46)–(49) are valid for both planar and cylindrical coordinates. To calculate the EDF in the cylindrical case, we have to average D over angles according to Eq. (40). Introducing cylindrical coordinates P and ϑ in the (p_θ, p_z) plane, we obtain, for the particularly simple case (49),

$$D_\varepsilon = \frac{(\omega_L \delta)^2}{R}\frac{m(\omega\delta)^2}{2}\sqrt{2m\varepsilon}\,Y\left[\frac{m(\omega\delta)^2}{2\varepsilon}\right], \tag{50}$$

where $Y(x)$ is defined as

$$Y(x) = \frac{1}{2}\int_0^{2\pi} d\vartheta \int_0^1 dP \frac{P^3\cos^2\vartheta(1-P^2\sin^2\vartheta)\sqrt{1-P^2}}{(1-P^2+x)^2}$$
$$= \frac{1}{16}\left(\frac{-23+15x}{3} - \frac{(-3-6x+5x^2)\arctan 1/\sqrt{x}}{\sqrt{x}}\right). \tag{51}$$

Expression (50) differs considerably from the energy diffusion coefficient

$$D_\varepsilon = \frac{(eE\lambda)^2 \nu^3}{6(\nu^2+\omega^2)}, \tag{52}$$

which describes Joule heating [3]. The principal difference is that Joule heating is local [the energy diffusion coefficient (52) is a function of the local value of the electric field], while non-Joule heating is nonlocal. The energy diffusion coefficient (50) is determined by the entire profile of the rf fields in the skin layer. Also, contrary to Eq. (52), D_ε in Eq. (50) does not depend explicitly on gas pressure: the collision frequency does not appear in Eq. (50). The energy diffusion coefficient (50) exhibits a maximum as a function of the product $\omega\delta$ and increases monotonically as a function of ε (see Fig. 8).

The EDF calculated from Eq. (39) with D_ε given by Eq. (50) is shown in Fig. 9. The EDF is found with neglect of the electrostatic potential in the plasma (rectangular potential well) and no Coulomb interactions among electrons. In a semilogarithmic plot versus energy, the EDF is concave at low energies and convex at high energies that can be characterized by three temperatures. The concave shape of the EDF at low energies is due to a decrease of the energy dif-

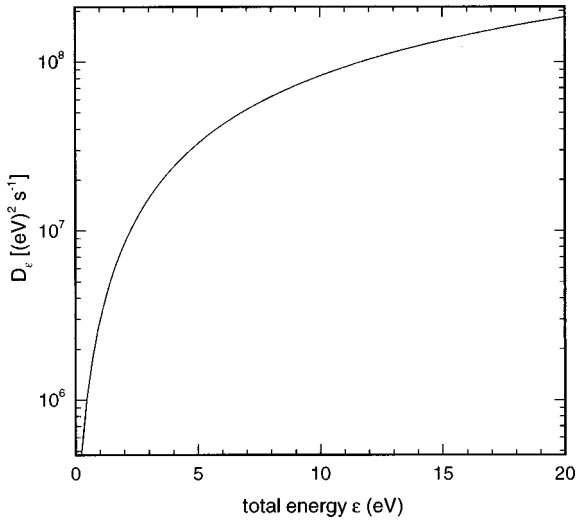

FIG. 8. Energy diffusion coefficient D_ε as a function of the total electron energy for a thin skin layer [Eq. (50)]. The discharge conditions are $\delta=1$ cm, $R=5$ cm, $B_0=2$ G, $\omega=8.5\times10^7$ s^{-1}, and a rectangular potential well for $\phi(r)$.

fusion coefficient with electron energy. The convex shape in the inelastic energy range $\varepsilon>\varepsilon^*$ is due to energy loss in inelastic collisions. Such three-temperature EDFs have recently been reported for ICPs in argon [28].

IV. PARTICLE-IN-CELL–DYNAMIC MONTE CARLO SIMULATION

The particle-in-cell–dynamic Monte Carlo simulation was employed to assess the electron-heating efficiency and to calculate the electron distribution function in weakly collisional regimes. The well-known particle-in-cell method [29,30] was used to ascribe particle attributes onto a grid. The simulations were performed for prescribed profiles of the fields.

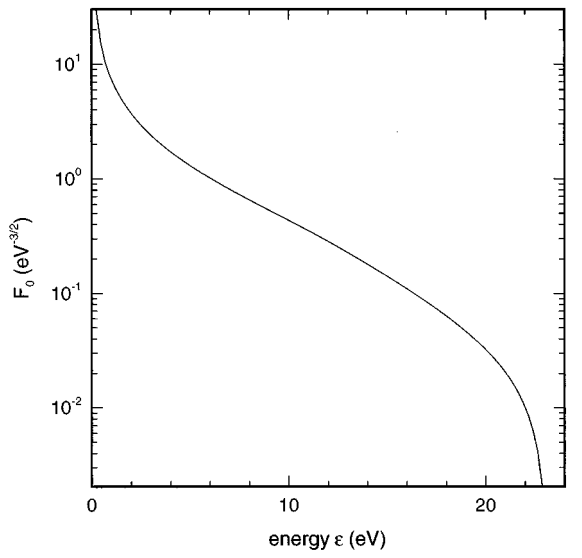

FIG. 9. EDF in argon calculated from Eq. (39) with the energy diffusion coefficient (50). The discharge conditions are the same as in Fig. 8.

Alternating electric and magnetic fields were taken in the form (11) and (12). The profile of the electrostatic potential was taken as $\phi(r)=\phi_0(r/R)^4$. An infinitely thin sheath with a potential drop $\Delta\phi=\phi_w-\phi_0$ was assumed to exist near the wall. The wall potential ϕ_w with respect to the plasma potential at the axis (equal to zero) was found self-consistently to equalize the number of ionizations and the number of electrons lost to the wall. The electron distribution function and the heating rate in a steady state were computed for different gas pressures and driving frequencies.

The collision processes are described using the DMC technique [31,32]. The DMC method has some advantages compared to the null-collision Monte Carlo method [33,34], which is widely used to calculate electron velocity distribution functions (EVDFs). The null-collision method requires the electron free-flight distribution as an input to the simulation. In contrast, the DMC method does not require knowledge of the free-flight distribution. In fact, the free-flight distribution is an output of the DMC simulation. In addition, the DMC method requires fewer random numbers per time step to describe the electron collision processes, as compared to the null-collision method. The DMC method is a transparent solution to the Boltzmann equation. The essence of the method consists in using the set of probability functions

$$\mathcal{P}_{ij}^{C}(v_0)=\Delta t n_j v_0 2\pi\int_0^{\pi}\sigma_{ij}(v_0,\chi')\sin\chi' d\chi', \tag{53}$$

$$\mathcal{P}_{ij}^{v}(v|v_0)=\delta(u-g(v_0,\varepsilon_{ij},\chi)), \tag{54}$$

$$\mathcal{P}_{ij}^{\chi}(\chi|v_0)=\sigma_{ij}(v_0,\chi)\sin\chi\Big/\int_0^{\pi}\sigma_{ij}(v_0,\chi')\sin\chi' d\chi', \tag{55}$$

where $\mathcal{P}_{ij}^{C}$, $\mathcal{P}_{ij}^{v}$, and $\mathcal{P}_{ij}^{\chi}$ correspond to the electron collision probability, the conditional probability for an electron to have speed v after collision, and the probability for an electron to be scattered into angle χ, respectively. The index i represents the collision process (i.e., excitation, ionization, etc.) that involves an electron and a particle j that has a collision cross section $\sigma_{ij}(v_0,\chi)$, a function of electron speed before the collision v_0, and the scattering angle χ. The heavy species are assumed motionless. The δ function in Eq. (54) ensures that momentum and energy are both conserved during the collision. These conservation laws require the postcollision electron speed to be

$$g(v_0,\varepsilon_{ij},\chi)=\left[v_0^2\left(1-\frac{2m}{m_j}(1-\cos\chi)\right)-\frac{2\varepsilon_{ij}}{m}\right]^{1/2}, \tag{56}$$

where m is the mass of the electron, m_j is the mass of particle j, and ε_{ij} is the energy lost by the electron in the collision of type i with particle j. The free motion of the electrons (i.e., the flight of an electron between collisions) is described by explicitly integrating Newton's equations of motion

$$\mathbf{v}(t_0+\Delta t)=\mathbf{v}(t_0)+\frac{1}{m}\int_{t_0}^{t_0+\Delta t}\mathbf{F}(t)dt, \tag{57}$$

TABLE I. Energy lost in inelastic collisions $\mathcal{E}_{\rm in}$ energy carried to the wall $\mathcal{E}_w$ (per electron in a unit time), and the ratio of electron escapes to the number of inelastic collisions κ for different pressures and driving frequencies at $B=1$ G.

Frequency (MHz) \ Pressure	0.3 mtorr			1 mtorr			10 mtorr		
	$\mathcal{E}_{\rm in}$ (10^{-13}) W	$\mathcal{E}_w$ (10^{-13})	κ (%)	$\mathcal{E}_{\rm in}$ (10^{-13}) W	$\mathcal{E}_w$ (10^{-13}) W	κ (%)	$\mathcal{E}_{\rm in}$ (10^{-13}) W	$\mathcal{E}_w$ (10^{-13}) W	κ (%)
2	2.2	2.5	2.8	5.7	6.3	2.9	1.6	0.37	0.35
13.56	1.45	1.54	2.1	2.3	1.9	1.3	6.1	3.8	0.43
40.7	1.1	1.1	1.8	2.0	1.6	1.1	8.8	7.0	0.7

$$\mathbf{r}(t_0+\Delta t)=\mathbf{r}(t_0)+\int_{t_0}^{t_0+\Delta t}\mathbf{u}(t)dt, \tag{58}$$

where $\mathbf{v}$ and $\mathbf{r}$ are the electron velocity and position vector, respectively, t is the current time, Δt is a small time increment, and $\mathbf{F}$ is the force acting on the electrons.

An algorithm can now be devised based on Eqs. (53)–(55) to describe the collisional motion of an electron in a plasma. The probability that the electron will not suffer a collision is given by

$$\mathcal{P}^{\rm NC}=1-\sum_{i,j}\mathcal{P}_{ij}^{C}, \tag{59}$$

whereas the probability for a collision of type i (ionization, excitation, or elastic) with a particle j is given by Eq. (53). A random number $\mathcal{Y}$ uniformly distributed in the interval [0,1] dictates whether the electron suffers no collision

$$\mathcal{Y}\leqslant\mathcal{P}^{\rm NC} \tag{60}$$

or suffers a collision of type i with particle j,

$$\mathcal{P}^{\rm NC}+\sum_{l=1}^{k-1}\mathcal{P}_l^{C}\leqslant\mathcal{Y}\leqslant\mathcal{P}^{\rm NC}+\sum_{l=1}^{k}\mathcal{P}_l^{C}, \tag{61}$$

where each value of l corresponds to a unique pair (i,j). Once the collision type has been determined, the energy of the electron is revised according to the collision characteristics (e.g., elastic and inelastic), by using Eq. (54). The velocity of the electron is then updated based on the scattering and azimuthal angles, with probability distributions given by Eq. (55). For the simulation reported in this paper, only electron collisions with neutral atoms were considered and the scattering was assumed to be isotropic.

The chamber geometry studied here is axisymmetric. Advantage is taken of this symmetry, so that all quantities are functions of only one spatial coordinate (the radial position of a particle). However, the logic associated with the three-dimensional particle motion is exact [35]. Cylindrical coordinates are used to describe the electron motion in velocity space. During the PIC-DMC simulation all three electron velocity components (i.e., v_r, v_θ, and v_z) and two spatial coordinates (r and θ) are recorded. As electrons are moved forward in time, their velocity components are calculated at specific times of the rf cycle [phase angle $\xi=\omega t(\mathrm{mod}2\pi)$] and statistics are accumulated. Numerically, the time-dependent electron velocity distribution function $f(\mathbf{v},r,\xi)$ is computed on discrete volume elements $\Delta v_r\Delta v_\theta\Delta v_z\Delta r\Delta\xi$ located around the velocity $\mathbf{v}$, the radial position r, and the phase angle ξ. As the simulation advances in time, the appropriate (v_r,v_θ,v_z,r,ξ) bins of the EVDF are updated.

The particles were initially given positions and velocities chosen randomly. At the beginning of the simulation the wall potential was set to a relatively high value (exceeding the ionization threshold) to ensure that the electron ensemble will not decrease with time. Thereafter, the wall potential was adjusted periodically (every 10–80 rf cycles depending on conditions) to maintain a constant, within limits, number of electrons. The procedure was as follows. After an electron move, the new location of the electron was tested to determine whether the electron had reached the plasma boundary. Then, if the radial energy of the electron $mv_r^2/2$ was greater than the potential drop in the sheath $e\Delta\phi$, the electron was lost, otherwise it was specularly reflected. In between wall-potential adjustements statistics were collected with regard to the energy of the electrons striking the plasma boundary. The resulting vector reflected the electron energy distribution function (EEDF) of the electrons penetrating the sheath. The vector containing the electron energies was then sorted in ascending order. If the number of ionizations was not equal to the number of electrons escapes (highly likely) the wall potential was adjusted based on the net electron number change. If there was an electron number deficit the wall potential was set to a higher value to confine electrons. If $\mathcal{N}^-$ is the electron-number deficit, the new potential was determined by simply moving $\mathcal{N}^-$ notches up (with respect to energy) the EEDF sorted vector from the notch closest to the current wall potential. If there was an electron number surplus, the wall potential was set to a lower value to allow more electrons to escape. If $\mathcal{N}^+$ is the electron-number surplus, the new wall potential was determined by simply moving $\mathcal{N}^+$ notches down (with respect to energy) from the notch closest to the current wall potential. Naturally, this results in a wall potential that fluctuates with time. If the statistics are adequate, the wall potential fluctuations are kept to a minimum. After the establishment of a dynamic steady state, the characteristics of the electron ensemble were recorded to calculate the EDF and the ionization, loss, and heating rates.

V. RESULTS OF THE DMC SIMULATIONS

Argon-gas pressures in the range 0.1–10 mtorr, excitation frequencies in the range 2–40 MHz, and magnetic induction

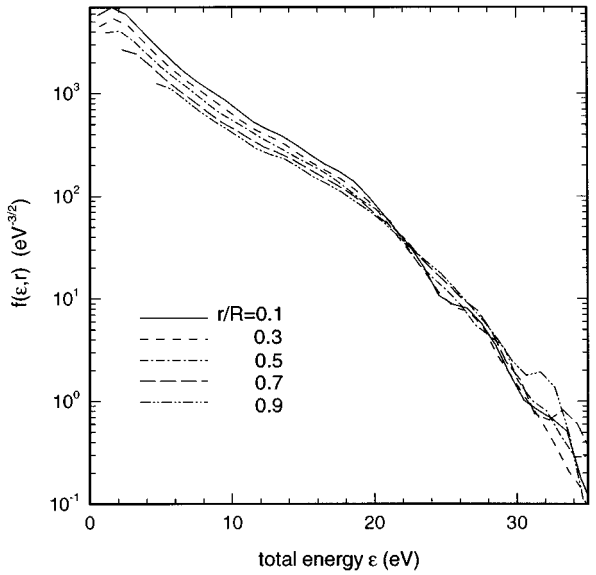

FIG. 10. EEDF from DMC simulations as a function of total energy ε for different radial positions, with an argon pressure of 1 mTorr, $B_0=1$ G (no skin effect), and $\omega=8.5\times10^7$ cm^{-3}. The electrostatic potential is $\phi(r)=\phi_0(r/R)^4$, where $\phi_0=5$ V.

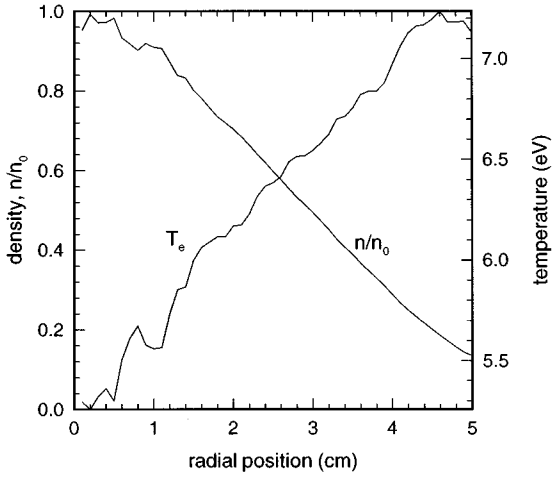

FIG. 11. Radial profiles of electron density and ''temperature'' for the conditions of Fig. 10. The radial increase of temperature corresponds to the concave EEDF in Fig. 10.

fields of 1 or 2 G were examined for a chamber radius $R=5$ cm. The results of simulations are summarized in Table I for the case of a low-density plasma with uniform inductive field $B=1$ G (no skin effect). One observes the following trends. For 13.56 and 40.7 MHz, the energy lost in inelastic collisions $\mathcal{E}_{\rm in}$ and the energy carried to the wall $\mathcal{E}_w$ both increase with increasing pressure. For 2 MHz there is a maximum of $\mathcal{E}_{\rm in}$ and $\mathcal{E}_w$ with respect to pressure. For 0.3 and 1 mtorr, $\mathcal{E}_{\rm in}$ and $\mathcal{E}_w$ decrease with an increase of ω, while at 10 mtorr $\mathcal{E}_{\rm in}$ and $\mathcal{E}_w$ increase with ω. The ratio of electron escapes to the number of inelastic collisions κ decreases with increasing pressure, except for the 2-MHz case. The higher the heating rate, the longer the EDF ''tail,'' and a larger part of energy is lost in collisions compared to energy carried to the wall. At higher pressures more energy is lost for excitation than for ionization.

Figure 10 shows the calculated EEDF as a function of total electron energy ε for different radial positions. The amplitude of time modulation of the EEDF in DMC simulations was found to be negligible, as expected for $\omega\gg\nu^*$. Namely, the EEDFs at different phases of the field ξ coincide with each other within the accuracy of the numerical simulation. The EEDFs shown in Fig. 10 are normalized according to

$$\int_{e\phi(r)}^{\infty} f\sqrt{\varepsilon-e\phi(r)}\,d\varepsilon=n_e(r)/n_0, \tag{62}$$

where $n_e(r)$ is the electron density at position r and n_0 is the electron density on the axis.

Figure 11 shows the radial profiles of electron density and temperature for the conditions of Fig. 10. The temperature increases towards the wall since the EEDF is concave in the elastic energy range, which contains most of the electrons [36].

Figure 12 shows the radial distribution of the rf current density for different field phases ξ [Fig. 12(a)] and the current density vs phase ξ at different r [Fig. 12(b)]. The current density is shifted with respect to the E_θ field by $\sim\pi/2$ as is expected for $\nu\ll\omega$. The phase shift does not depend significantly on the radial position. The radial distribution of the rf current does not show significant anomalies, which are typical of the anomalous skin effect [10,18]. Under these conditions, the distance a thermal electron travels during the field period, $l\sim v/\omega\approx1.4$ cm, is small compared to the characteristic scale of the E_θ field inhomogeneity, approximately equal to R. Significant current diffusion off the skin layer and formation of multiple current layers with a phase shift of the current density and the field are expected to occur at $l>\delta$ [18].

Figure 13 illustrates the anisotropy degree of the EDF. The dashed curve shows the distribution $f_z(\varepsilon_z,r)$ found by sampling electrons with a given energy $\varepsilon_z=mv_z^2/m$, parallel to the magnetic field regardless of v_r and v_θ. The solid curve shows the distribution $f_\perp(\varepsilon_\perp,r)$ perpendicular to the field, which was found by collecting electrons with given $v_r^2+v_\theta^2$ irrespective of the value of v_z. Both distributions f_z and $f_\perp$ are at $r=0.1R$. It is seen that f_z and $f_\perp$ are close to each other for trapped electrons, with $\varepsilon<e\phi_w$, but differ considerably for free electrons, with $\varepsilon>e\phi_w$. One may conclude that the EDF of trapped electrons is almost isotropic, while the EDF of free electrons is notably anisotropic. The tail of $f_\perp$ is strongly depleted due to the escape of electrons with $\varepsilon_\perp>e\phi_w$ to the wall as discussed in Sec. III.

Figure 14 shows the distribution $f_\perp(\varepsilon_\perp,r)$ at different radial positions. It is seen that the tail of the distribution decays with energy more rapidly near the axis, in accord with the discussion in Sec. III. Overall, the DMC simulation results corroborate the theory presented in earlier sections.

VI. DISCUSSION

Electron heating in a gas discharge is a two-step process that includes (a) electron interactions with electromagnetic fields and (b) transfer of the directed energy gained from the field into the energy of thermal motion. An electron can be

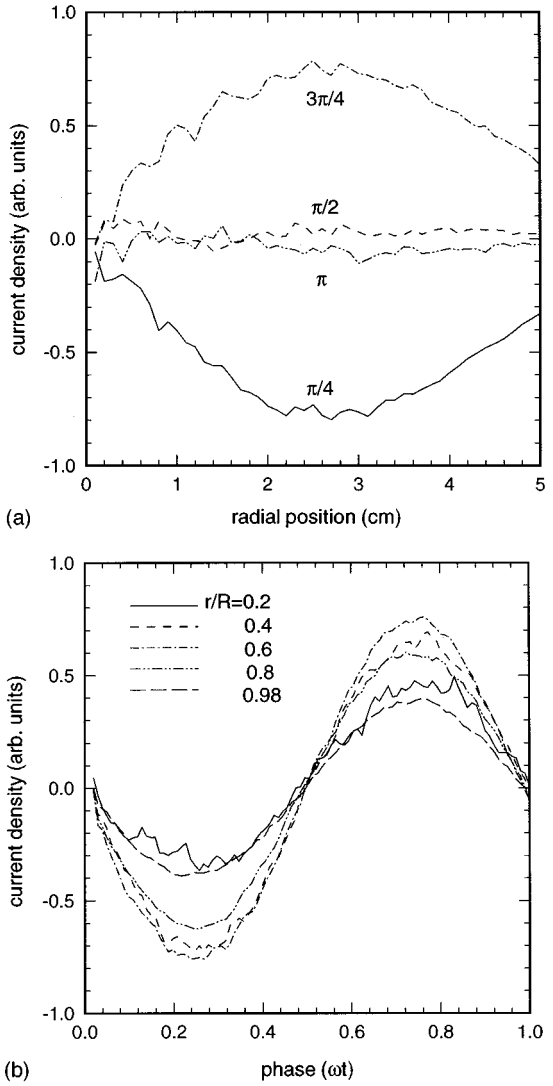

FIG. 12. Azimuthal rf current density versus (a) the radial position r for different phases of the rf field (labels near the curves) and (b) the field phases for different r. The discharge conditions are the same as in Fig. 10.

accelerated or decelerated by the electric field depending on whether it moves along or against the direction of the force. The result of successive interactions depends upon phase correlations. Collisions play a twofold role. They change the direction of the electron motion and thus (i) transfer directed kinetic energy acquired from the fields into kinetic energy of random motion and (ii) randomize the field phase between succesive interactions. The average energy gain per collision is the small net difference between large actual gains and losses. We have demonstrated that phase randomization can also occur without collisions so that collisionless heating exists in the ICP. The common feature of different heating regimes is the statistical nature of the heating. In all cases, heating represents a random walk of an electron along the energy axis, which is described in terms of diffusion (energy diffusion).

Joule heating dominates at high gas pressures when the fields do not change appreciably over the mean free path of electrons. The Joule heating is therefore local; processes (a) and (b) referred to above take place at the same point and the

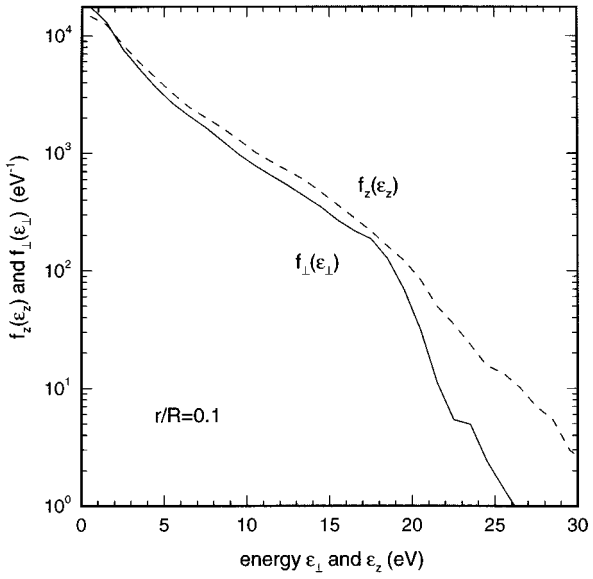

FIG. 13. Electron distributions $f_\perp(\varepsilon_\perp, r)$ (solid line) and $f_z(\varepsilon_z, r)$ (dashed line) at $r = 0.1R$. The discharge conditions are the same as in Fig. 10.

heating rate is determined by the local value of the electric field. The energy diffusion coefficient given by Eq. (52) is the product of a single kick in energy $\Delta\varepsilon = (eE_{\text{eff}}\lambda)^2$ and the frequency of collisions ν. When the electron mean free path exceeds the thickness of the rf sheath or the skin layer, electron heating becomes nonlocal. The processes of electron interaction with rf fields and ''randomizing collisions'' are now separated in space. When the electron mean free path exceeds the discharge dimensions ''collisions'' with plasma boundaries (potential barriers) occur more frequently than collisions with gas species. The finite dimensions of the plasma become an important consideration under these conditions since phase correlations of the rf fields could result in large energy excursions compared to the energy change in the single interaction with the rf sheath or skin layer. On the

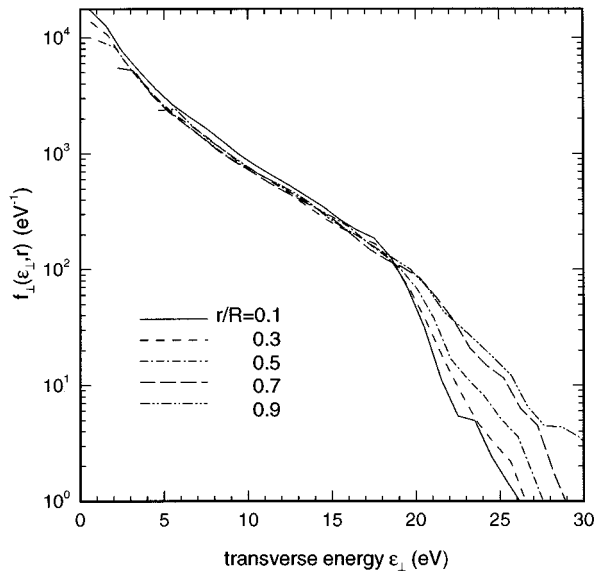

FIG. 14. Electron distribution $f_\perp(\varepsilon_\perp, r)$ for different radial positions. The discharge conditions are the same as in Fig. 10.

other hand, under certain conditions, electron dynamics becomes chaotic even without collisions with particles. The entire discharge volume participates in the heating process under these nonlocal conditions even though the heating fields are clearly localized. The heating regime where electron interactions with the rf field and collisions are spatially separated is referred to as non-Joule heating.

We have further distinguished collisionless and hybrid heating regimes as belonging to non-Joule heating. The specific feature of collisionless heating is that it can impart energy into one direction. However, if the heating process is slow compared to collisions (as it typically occurs in gas discharges), the EDF should be almost isotropic.

An analysis of electron heating and formation of the EDF requires simulations of electron kinetics on a long time scale compared to the period of the rf field, the bounce time, and the intercollision time $1/\nu$. The electron energy spectrum is established on a time scale that is of the order of the energy relaxation time $\sim 1/\nu^*$. During its lifetime, an average electron undergoes many elastic collisions. Moreover, during its lifetime, an average electron must generate one electron-ion pair to maintain a steady state. The fields in a discharge are established in such a way that during their lifetime slow electrons are heated up to energy $\sim e\phi_w$. The shape of the EDF is determined by a balance of electron fluxes along the energy axis. Heating produces a duffusive flux of electrons from the low-energy region where particles are abundant to the high-energy region where the particle density is low. Inelastic collisions produce a sink of electrons at high energies and a source of electrons at low energies. In the absence of Coulomb interactions, the EDF may substantially differ from a Maxwellian.

The oscillatory magnetic field has a large impact on collisionless electron heating. The Lorentz force changes the direction of electron diffusion in velocity space. In the hybrid regime, however, the influence of the B field is not so critical. In fact, DMC simulations of low-density ICP (no skin effect) with and without the B field reveal a surprisingly small difference in the heating rate at a frequency 13.56 MHz and argon pressure 1 mtorr. With a decrease of ω, the influence of the B field may become more important. If we assume that the same electric field E_θ is required to sustain a discharge for different ω, then a larger rf current and B field would be necessary at lower ω since $E_\theta \propto \omega B$. The higher B field produces higher ''radiation pressure,'' preventing electrons from entering the skin layer of high E_θ. Thus, at lower ω the heating rate with account of the B field should be lower than that without the B field. This was in fact observed in our simulations.

The heating rate and the electron energy spectrum depend on the entire profiles of electromagnetic and electrostatic fields in the discharge. A pronounced skin effect, together with weak Coulomb interactions among electrons, results in the following phenomenon. Due to the presence of the electrostatic potential in the plasma, slow electrons are confined in the vicinity of the potential maximum near the discharge center. These electrons cannot reach the skin layer near the wall and be heated. In the absence of Coulomb interactions, the mean energy of these electrons can be very low and a sharp peak of the EDF can be formed at low energies (see Fig. 15). This phemonenon is well known for CCPs [37,27,38] and has been recently reported for ICPs at low-power input (hence relatively low plasma density where Coulomb interactions are not too strong) [28]. Manifestation of the nonlocal electron kinetics is therefore rather common for all low-pressure plasmas regardless of the particular mechanism of electron heating and discharge maintenance.

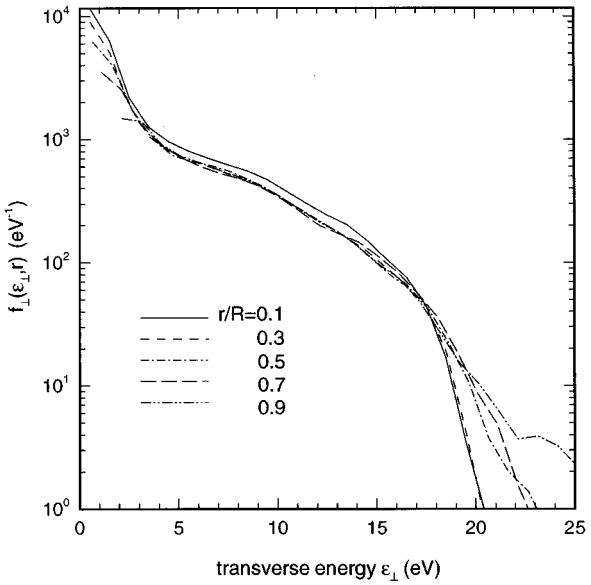

FIG. 15. Electron distribution $f_\perp(\varepsilon_\perp, r)$ for a thin skin layer: $\delta = R/5$, $B_0 = 2$ G, and $\omega = 8.5 \times 10^7$ s^{-1}.

VII. CONCLUSION

We have studied electron kinetics in a nearly collisionless cylindrical ICP taking into account the influence of the oscillatory magnetic field and the finite dimensions of the plasma. An analysis of single-particle dynamics revealed that electron motion may become chaotic even without collisions with gas particles. We have distinguished collisionless heating from hybrid heating. In the hybrid heating regime, collisions with particles are important for randomization of electron motion. We have developed a nonlocal approach to the solution of the electron Boltzmann equation in a free-flight regime when the traditional two-term Legendre expansion is not valid. We have calculated the energy diffusion coefficient for hybrid heating regimes and identified resonance phenomena caused by the finite dimensions of the plasma. We have used the Dynamic Monte Carlo simulations to calculate the EDF in a wide range of discharge conditions. The results of the DMC simulations have been compared to theoretical analysis. Our studies indicate that the EDF of trapped electrons with total energy below the wall potential is almost isotropic and is a function solely of total energy ε, while the EDF of free electrons with $\varepsilon > e\phi_w$ is notably anisotropic and depends on the radial position.

ACKNOWLEDGMENTS

We are grateful to V.A. Godyak, A.J. Lichtenberg, and L.D. Tsendin for reading and commenting on the manuscript. This work was supported in part by NSF Grant No. CTS-9216023.

[1] M. A. Lieberman and A. J. Lichtenberg, *Principles of Plasma Discharges and Materials Processing* (Wiley, New York, 1994).
[2] H. U. Eckert, in *Proceedings of the Second International Conference on Plasma Chemical Technology, San Diego, 1984*, edited by H. V. Boenig (Technomic, Lancaster, 1986).
[3] V. I. Kolobov and W. N. G. Hitchon, Phys. Rev. E **52**, 972 (1995).
[4] U. Kortshagen, I. Pukropski, and L.D. Tsendin, Phys. Rev E **51**, 6063 (1995).
[5] V. I. Kolobov, G. J. Parker, and W. N. G. Hitchon, Phys. Rev. E **53**, 1110 (1996).
[6] V. A. Godyak, Zh. Tekh. Fiz. **41**, 1364 (1971) [Sov. Phys. Tech. Phys. **16**, 1073 (1972)].
[7] C. E. Goedde, A. J. Lichtenberg, and M. A. Lieberman, J. Appl. Phys. **64**, 4375 (1988).
[8] J. Hopwood, C. R. Guarnieri, S. J. Whitehair, and J. J. Cuomo, J. Vacuum Sci. Technol. **11**, 147 (1993).
[9] V. A. Godyak, R. B. Piejak, and B. M. Alexandrovich, Plasma Sources Sci. Technol. **3**, 169 (1994).
[10] M. M. Turner, Plasma Sources Sci. Technol. **5**, 159 (1996).
[11] V. Vahedi, M. A. Lieberman, G. DiPeso, T. D. Rognlien, and D. Hewett, J. Appl. Phys., **78**, 1446 (1995).
[12] H. A. Blevin, J. A. Reinolds, and P. C. Thonemann, Phys. Fluids **16**, 82 (1973).
[13] I. D. Kaganovich, V. I. Kolobov, and L. D. Tsendin, Appl. Phys. Lett. **69**, 3818 (1996).
[14] R. A. Demirkhanov, I. Ya. Kadysh, and Yu. S. Khodyrev, Zh. Eksp. Teor. Fiz. **46**, 1169 (1964) [Sov. Phys. JETP **19**, 791 (1964)].
[15] R. H. Cohen and T. D. Rognlien, Plasma Sources Sci. Technol. **5**, 442 (1996).
[16] M. R. Gibbons and D. W. Hewett, J. Comput. Phys. **120**, 231 (1995).
[17] H. A. Blevin, J. M. Greene, D. L. Jolly, and R. G. Storer, J. Plasma Phys. **10**, 337 (1973).
[18] V. I. Kolobov and D. J. Economou, Plasma Sources Sci. Technol. (to be published).
[19] K. Henjes, J. Appl. Phys. **79**, 21 (1995).
[20] K. Chandrakar, J. Phys. D **11**, 1809 (1978).
[21] G. Schmidt, *The Physics of High-Temperature Plasmas* (Addison-Wesley, Reading, MA, 1966).
[22] E. S. Weibel, Phys. Rev. **114**, 18 (1959).
[23] R. Z. Sagdeev, D. A. Usikov, and G. M. Zaslavsky, *Nonlinear Physics from the Pendulum to Turbulence and Chaos* (Harwood Academic, Chur, Switzerland, 1988).
[24] A. J. Lichtenberg and M. A. Lieberman, *Regular and Chaotic Dynamics* (Springer-Verlag, New York, 1992).
[25] V. L. Ginzburg and A. V. Gurevich, Usp. Fiz. Nauk **70**, 201 (1960) [Sov. Phys. Usp. **3**, 115 (1960)].
[26] L. D. Tsendin and Yu. B. Golubovskii, Zh. Tekh. Fiz. **47**, 1839 (1977) [Sov. Phys. Tech. Phys. **22**, 1066 (1977)].
[27] I. D. Kaganovich and L. D. Tsendin, IEEE Trans. Plasma Sci. **20**, 86 (1992).
[28] V. A. Godyak, R. B. Piejak, and B. M. Alexandrovich, in *Proceedings of the ICOPS'96, Boston, 1996* (IEEE, 1996).
[29] R. W. Hockney and J. W. Easwood, *Computer Simulation using Particles* (Hilger, Bristol, 1988).
[30] C. K. Birdsall and A. B. Langdon, *Plasma Physics via Computer Simulation* (McGraw-Hill, New York, 1985).
[31] D. P. Lymberopoulos and J. D. Shieber, Phys. Rev. E **50**, 4911 (1994).
[32] D. P. Lymberopoulos and D. J. Economou, J. Phys. D **28**, 727 (1995).
[33] H. R. Skulerud, J. Phys. D **25**, 1567 (1968).
[34] Y. Weng and M. J. Kushner, Phys. Rev. A **42**, 6192 (1990).
[35] G. A. Bird, *Molecular Gas Dynamics and the Direct Simulation of Gas Flows* (Oxford Science, New York, 1994).
[36] V. I. Kolobov and V. A. Godyak, IEEE Trans. Plasma Sci. **23**, 503 (1995).
[37] V. A. Godyak and R. B. Piejak, Phys. Rev. Lett. **65**, 996 (1990).
[38] U. Buddemeier, U. Kortschagen, and I. Pukropski, Appl. Phys. Lett. **67**, 191 (1995).